Wang and Yang
Protection and Control of Modern Power Systems (2023) 8:40
https://doi.org/10.1186/s41601-023-00315-9

Protection and Control of
Modern Power Systems

ORIGINAL RESEARCH Open Access

Optimal PV array reconfiguration under partial shading condition through dynamic leader based collective intelligence

Yutong Wang[1] and Bo Yang[1*]

Abstract

This paper applies the innovative idea of DLCI to PV array reconfiguration under various PSCs to capture the maximum output power of a PV generation system. DLCI is a hybrid algorithm that integrates multiple meta-heuristic algorithms. Through the competition and cooperation of the search mechanisms of different metaheuristic algorithms, the local exploration and global development of the algorithm can be effectively improved to avoid power mismatch of the PV system caused by the algorithm falling into a local optimum. A series of discrete operations are performed on DLCI to solve the discrete optimization problem of PV array reconfiguration. Two structures (DLCI-I and DLCI-II) are designed to verify the effect of increasing the number of sub-optimizers on the optimized performance of DLCI by simulation based on 10 cases of PSCs. The simulation shows that the increase of the number of sub-optimizers only gives a relatively small improvement on the DLCI optimization performance. DLCI has a significant effect on the reduction in the number of power peaks caused by PSC. The PV array-based reconstruction system of DLCI-II is reduced by 4.05%, 1.88%, 1.68%, 0.99% and 3.39%, when compared to the secondary optimization algorithms.

Keywords PV array reconfiguration, Partial shading condition, Dynamic leader based collective intelligence, Maximum power extraction, Total-cross-tied

1 Introduction

Consumption of energy has led to the rapid depletion of fossil fuels such as coal, oil and natural gas, and serious environmental pollution. These bring huge challenges [1, 2]. To cope with the approaching energy crisis, there is a need to change from fossil energy to low-carbon and clean renewable energy [3]. As one of the most promising renewable energies, solar energy has been widely promoted and applied [4]. However, photovoltaic (PV) systems in practical engineering application still face many problems that need to be solved [5]. For example, PV systems are sensitive to changes in the external environment [6]. When the temperature and irradiance changes rapidly, a PV system will generate a large mismatched power loss [7]. In particular, when PV systems are in a partial shading condition (PSC), multiple power peaks can appear in the *P*–*V* characteristic curves of the arrays [8], resulting in a hot spot effect and causing PV panels to burn out because of local uneven heating [9].

In practical engineering application, PSC is a relatively common phenomenon [10]. At present, many methods with excellent performance have been applied to solve various problems of the systems in PSC, e.g., parallel bypassed diodes on the PV panels [11] and performing maximum power point tracking (MPPT) for the output power [12]. However, previous studies have shown that

*Correspondence:
Bo Yang
yangbo_ac@outlook.com
[1] Faculty of Electric Power Engineering, Kunming University of Science and Technology, Kunming 650500, China

the multi-peak nature of the PV panel itself can lead to power mismatch loss in the connected bypass diodes [10]. Also, there are huge implementation and control costs when MPPT technology is applied to large-scale PV power plants [13].

To reduce the power loss under PSC, PV reconstruction technology has become a research hotspot. The technology can be divided into static and dynamic reconstruction [14]. The former changes the physical location of PV components instead of the electrical connection [15], such as Sudoku, Rubik's cube, and column index technology. From this, a method of PV array reconfiguration is proposed for PV systems in different PSCs [13]. This is considered to be the perfect method for capturing the maximum power output of PV systems in different PSCs. As mentioned, it can be divided into static or dynamic reconfiguration depending on whether the electrical interconnect is changed [16]. Dynamic reconfiguration shows strong optimization performance for various PSCs that change rapidly in practical engineering. Many topologies have been proposed and widely used in dynamic reconfiguration. The more common forms are series-parallel, bridge-link, TCT, Suduku, etc [17]. In addition, some meta-inspiration algorithms have also been applied to the PV array reconfiguration, such as genetic algorithms (GA) [18], particle swarm optimization (PSO) [19], and butterfly optimization algorithms (BOA) [20], which can capture the maximum output power of PV arrays under dynamic and variable PSCs for TCT topology. However, these meta-inspiration algorithms easily fall into local optima because of the inherent defects of strong randomness [21].

To extract the maximum power of PV power plants in various PSCs, a novel PV array reconfiguration method based on dynamic leader-based collective intelligence (DLCI) is proposed here. A 9×9 TCT PV array reconstruction model is tested in various environments. The main innovations/contributions of the proposed method are:

- Compared to using a single meta-heuristic algorithm, DLCI with multiple sub-optimizer search mechanisms can maximize the optimization performance of the sub-optimizer.
- Through the competition and cooperation between different sub-optimizers, the convergence stability of the DLCI can be significantly improved, thereby greatly reducing the power fluctuation of a PV system during the reconstruction process.
- DLCI has higher convergence speed and accuracy, and can guide other sub-optimizers at a deeper level by selecting the currently obtained optimal sub-optimizer as the dynamic leader. Therefore, the global maximum power point (GMPP) can be obtained with a higher probability by using DLCI for PV array reconfiguration under PSC.
- To verify the effectiveness of the proposed method, a hardware-in-the-loop experiment is conducted, and the results of MATLAB and hardware-in-the-loop tests are compared and analyzed.

The structure of the paper is as follows: Sect. 2 describes the mathematical model of PV reconfiguration, and Sect. 3 designs the DLCI algorithm. Section 4 presents the design scheme of TCT array reconfiguration based on DLCI, while Sect. 5 conducts case analysis and research. In Sect. 6, the hardware-in-the-loop experiment is employed. Section 7 provides some discussion, and Sect. 8 gives a summary and perspective for the whole work.

2 TCT PV array reconfiguration modelling

2.1 TCT connected PV arrays

A PV cell is composed of a light generated current source, a parallel diode and a series resistor. Generally, PV cells are combined to form PV modules, which provide the required output power through series and parallel combinations [17]. The schematic diagram of a PV cell is shown in Fig. 1 [22]. Assuming that N_s and N_p are the numbers of PV cells in series and in parallel, respectively, the relationship between the output current and voltage is given as [22]:

$$I_{pv} = N_p I_g - N_p I_s \left(\exp\left[\frac{q}{AkT_c} \left(\frac{V_{pv}}{N_s} + \frac{R_s I_{pv}}{N_p} \right) \right] - 1 \right) - \left(\frac{N_p V_{pv}}{N_s} + R_s I_{pv} \right) / R_{SH} \tag{1}$$

$$I_g = (I_{sc} + k_i (T_c - T_{ref})) \frac{s}{1000} \tag{2}$$

$$I_s = I_{RS} \left[\frac{T_c}{T_{ref}} \right]^3 \exp\left[\frac{qE_g}{Ak} \left(\frac{1}{T_{ref}} - \frac{1}{T_c} \right) \right] \tag{3}$$

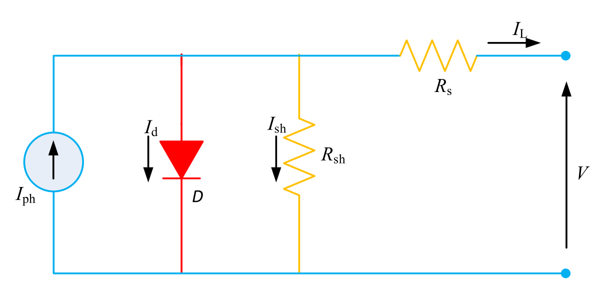

Fig. 1 Schematic diagram of a PV cell

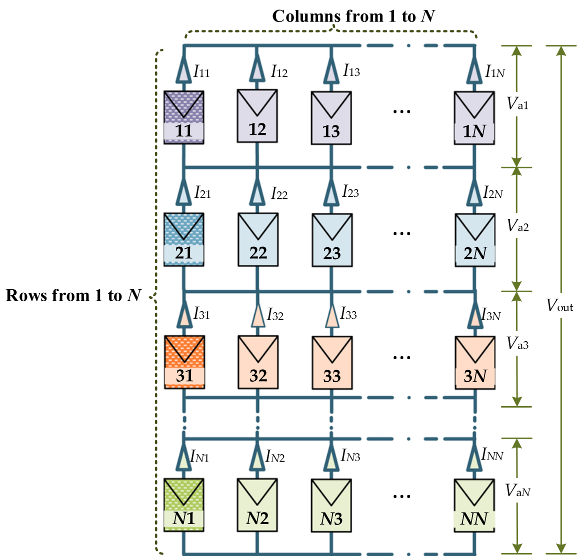

Fig. 2 $N\times N$ TCT connected PV array

where the description of each symbol is in the Nomenclature. It can be seen that the current generated by the PV array depends on both solar irradiance and temperature.

TCT structure is a common PV array topology in practical engineering. In this structure, PV arrays in each row are connected in parallel, and then PV arrays in each column are connected in series. For example, an $N\times N$ TCT interconnected PV array is shown Fig. 2. The output voltage of the entire PV array and the sum of current across each column of the PV array can be described as [23]:

$$V_{\mathrm{D}} = \sum_{p=1}^{F} V_{\mathrm{a}p} \tag{4}$$

$$I_{\mathrm{D}} = \sum_{q=1}^{F} \left(I_{pq} - I_{(p+1)q}\right) = 0, p = 1, 2, \ldots, 9, \mathrm{A}, \ldots, \mathrm{F} \tag{5}$$

where V_{ap} is the maximum voltage,and I_{pq} denotes the output current.

2.2 Performance evaluation

To evaluate the optimization performance of DLCI applied to PV array reconfiguration, three evaluation indicators are introduced, as [24]:

$$\mathrm{FF} = \frac{P_{\mathrm{PSC}}}{V_{\mathrm{OC}} \times I_{\mathrm{SC}}} \tag{6}$$

$$\Delta P_{\mathrm{MMPL}} = P_{\mathrm{STC}} - P_{\mathrm{PSC}} \tag{7}$$

$$\eta(\%) = \frac{P_{\mathrm{PSC}}}{P_{\mathrm{STC}}} \tag{8}$$

where P_{STC} is the maximum output power in the standard condition, which is defined as a solar irradiation of 1000 W/m^2 and an operational temperature of 25 ℃. P_{PSC} is the maximum output power in the PSC, V_{OC} is the open-circuit voltage, I_{SC} is the short circuit current, and ΔP_{MMPL} is the short circuit current, is the mismatched power loss.

3 Dynamic leader

3.1 Principle of DLCI

DLCI is a hybrid algorithm that integrates different search mechanisms of multiple meta-heuristics [22]. Each algorithm is defined as a sub-optimizer, and optimal search is carried out through cooperation and competition between different sub-optimizers. Each sub-optimizer can independently perform the optimization search in each iteration, and the sub-optimizer that obtains the optimal solution will be defined as a dynamic leader. In the following iteration, the leader will pass the obtained optimal solution and optimal fitness value to other sub-optimizers to guide them at a deeper level.

Generally, because of the diversity of search, a large number of sub-optimizers will lead to higher quality optimization, though the computing time will be too long. To verify the effect of increasing the number of sub-optimizers on the optimization performance of DLCI, two structures of DLCI are designed, i.e., a DLCI-I composed of grey wolf optimizer (GWO) [25], whale optimization algorithm (WOA) [26], and moth-flame optimization (MFO) [27], and a DLCI-II composed of GWO [25], WOA [26], MFO [27], artificial bee colony (ABC) [28], and PSO [19], as shown in Fig. 3.

3.1.1 Solution initialization

The initial population of DLCI can be described by:

$$X_{ij} = \mathrm{rand} \times \left(UB_j - LB_j\right), i = 1, 2, \ldots, Nj = 1, 2, \ldots, \mathrm{Dim} \tag{9}$$

where X_{ij} is the ith candidate solution with dimension j, N is the total number of candidate solutions (population number), Dim denotes the dimension size of the problem and rand is a random number. LB_j and UB_j are the jth lower bound and upper bound of the given problem, respectively.

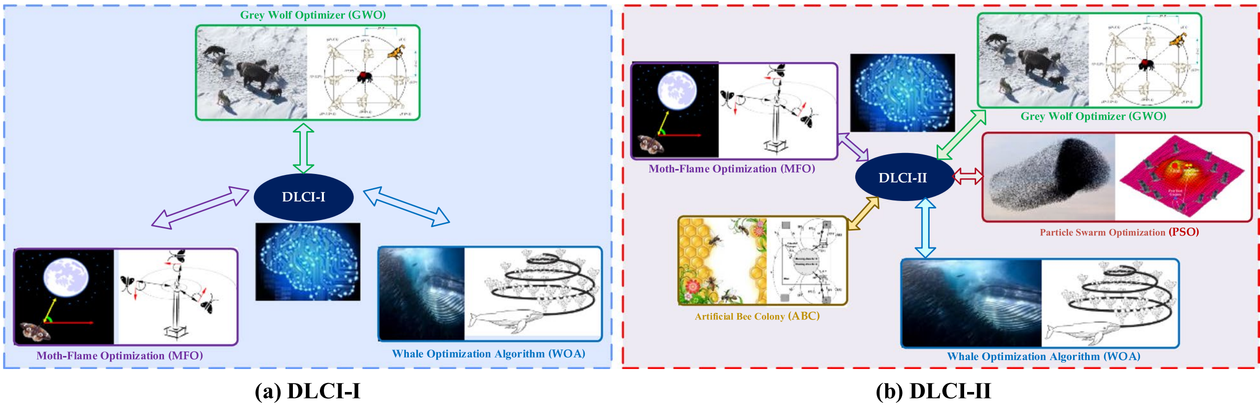

Fig. 3 Optimization framework: **a** Structure of DLCI-I; **b** Structure of DLCI-II

3.1.2 Mathematical model of DLCI-I and DLCI-II

(1) Selection of sub-optimizer.

The main operating mechanism of each sub-optimizer is described as follows.

- *GWO*: Gray wolves based on hunting strategy to update their positions, which can be described as [25]:

$$\begin{cases} \vec{X}_1 = \vec{X}_\alpha - \vec{A}_1 \cdot \left(\vec{D}_\alpha\right) \\ \vec{X}_2 = \vec{X}_\beta - \vec{A}_2 \cdot \left(\vec{D}_\beta\right) \\ \vec{X}_3 = \vec{X}_\delta - \vec{A}_3 \cdot \left(\vec{D}_\delta\right) \end{cases} \tag{10}$$

$$\begin{cases} \vec{D}_\alpha = \left|\vec{C}_1 \cdot \vec{X}_\alpha - \vec{X}\right| \\ \vec{D}_\beta = \left|\vec{C}_2 \cdot \vec{X}_\beta - \vec{X}\right| \\ \vec{D}_\delta = \left|\vec{C}_3 \cdot \vec{X}_\delta - \vec{X}\right| \end{cases} \tag{11}$$

$$\vec{X}(k+1) = \frac{\vec{X}_1 + \vec{X}_2 + \vec{X}_3}{3} \tag{12}$$

where k represents the number of iterations. $\vec{A}_1$, $\vec{A}_2$, $\vec{A}_3$, $\vec{C}_1$, $\vec{C}_2$ and $\vec{C}_3$ are coefficient vectors, while $\vec{X}_\alpha$, $\vec{X}_\beta$, $\vec{X}_\delta$ represent the position vectors of α wolf, β wolf and δ wolf, respectively. $\vec{X}$ represents the location vectors of other gray wolves.

- *WOA*: Humpback whales update their individual positions with a 50% probability by shrinking prey circles and spiral shaped path simultaneously, as [26]:

$$\begin{cases} \vec{D} = \left|\vec{C} \cdot \vec{X}^*(k) - \vec{X}(k)\right| \\ \vec{D'} = \left|\vec{X}^*(k) - \vec{X}(k)\right| \end{cases} \tag{13}$$

$$\vec{X}(k+1) = \begin{cases} \vec{X}^*(k) - \vec{A} \cdot \vec{D}, & p < 0.5 \\ \vec{D'} \cdot e^{bl} \cdot \cos(2\pi l) + \vec{X}^*(k), & p \geq 0.5 \end{cases} \tag{14}$$

where $\vec{A}$ and $\vec{C}$ are the coefficient vectors, $\vec{X}^*(k)$ is the optimal position vector of the whale in the kth iteration, and $\vec{X}(k)$ represents the position vector of the whale in the kth iteration. The constant b is used to define the shape of the spiral, l is a random number between $[-1, 1]$, and p is a random number between $[0, 1]$.

- *MFO*: The update mechanism of the moth position is selected as a logarithmic spiral, as [27]:

$$N_f(k) = \text{round}\left(N_f^{\max} - k * \frac{N_f^{\max} - 1}{k_{\max}}\right) \tag{15}$$

$$\vec{D}_i = \left|\vec{F}_j(k) - \vec{X}_i(k)\right| \tag{16}$$

$$\vec{X}_i(k+1) = \vec{D}_i \cdot e^{bl} \cdot \cos(2\pi l) + \vec{F}_j(k) \tag{17}$$

where the meanings of N_f, $N_f^{\max}$, $k_{\max}$, $\vec{F}_j$, and $\vec{X}_i$ can be found in the Nomenclature.

- *ABC*: The process of bee colony searching for optimal honey bee (food source) is as follows [28]:
First, scout bees search for the domain food source (domain solution) to generate a new food source (preferable solution), as:

$$\vec{X}_{id}(k+1) = \vec{X}_{id}(k) + \varnothing_{id}\left(\vec{X}_{id}(k) - \vec{X}_{hd}(k)\right) \tag{18}$$

where $\vec{X}_{id}$ represents the dth dimension position, and d is the dimension. h represents a randomly selected bee, and $\varnothing_{id}$ represents a uniformly distributed random number in [− 1, 1].

Employed bees search the domain according to the food source information shared by scout bees, and select the next food source based on the information [29, 30]. The probability of the ith bee being selected is calculated by:

$$p_i(k) = 0.9 \times \frac{\max_{j=1,2,..,N} f_j(k) - f_i(k)}{\max_{j=1,2,..,N} f_j(k) - \min_{j=1,2,..,N} f_j(k)} + 0.1 \tag{19}$$

where f_j represents the fitness function of the ith bee, and N represents the population size.

After the target food source is determined, employed bees can update their position according to (18). The search strategy of the scout bees is described by:

$$\vec{X}_i(k+1) = \overrightarrow{X^{\min}} + r \cdot \left(\overrightarrow{X^{\max}} - \overrightarrow{X^{\min}}\right) \tag{20}$$

where $\overrightarrow{X^{\min}}$ and $\overrightarrow{X^{\max}}$ are the minimum and maximum position vectors, respectively, where as r is a random number within [0, 1].

- *PSO*: In each iteration, each particle updates its velocity and position as:

$$\vec{V}_i(k+1) = \omega\vec{V}_i(k) + c_1r_1\left(\vec{P}_i(k) - \vec{X}_i(k)\right) + c_2r_2\left(\vec{G}(k) - \vec{X}_i(k)\right) \tag{21}$$

$$\vec{X}_i(k+1) = \vec{X}_i(k) + \vec{V}_i(k+1) \tag{22}$$

where $\vec{V}_i$ is the velocity vector, and ω represents the inertia weight. c_1 and c_2 represent the learning parameters, while r_1 and r_2 represent the random numbers between [0,1]. $\vec{P}_i$ is the individual best position, and $\vec{G}$ is the global best position of the whole swarm.

(B) Guiding strategy based on the dynamic leader.

The selection of dynamic leaders with the optimal solution is modelled as:

$$L = \arg \max_{o=1,2,\ldots,n} f_o^{\text{best}}(k) \tag{23}$$

where L represents the dynamic leader, f_o^{best} is the fitness function of the oth sub-optimizer, and n represents the number of sub-optimizers.

The guiding strategy based on the dynamic leader is described by (21). However, executing the guiding strategy too frequently will reduce the efficiency and stability of the DLCI. Therefore, the sub-optimizer is set to execute a guiding strategy after three iterations, as:

$$\vec{X}_o^{\text{worst}}(k) = \begin{cases} \vec{X}_L^{\text{best}}(k), & if\ \frac{k}{3} \in Z \\ \vec{X}_o^{\text{worst}}(k), & otherwise \end{cases} \tag{24}$$

where $\vec{X}_o^{\text{worst}}$ is the poor solution obtained by the oth sub-optimizer in the kth iteration, $\vec{X}_L^{\text{best}}$ is the optimal solution obtained by the dynamic leader in the kth iteration, and $\boldsymbol{Z}$ is the set of all integers.

3.2 Discrete design of DLCI-I and DLCI-II

DLCI was originally used to solve continuous optimization problems. For its excellent performance to be applied to discrete optimization problems, such as PV array reconfiguration, a series of discrete operations need to be performed as follows [31, 32].

(1) Discretization of initial population.

First, the initial population $\boldsymbol{N}$ of TCT PV array reconfiguration is discretized, and can be described as:

$$\boldsymbol{N} = \{[\boldsymbol{B}]_1, [\boldsymbol{B}]_2, [\boldsymbol{B}]_3, \ldots, [\boldsymbol{B}]_{n_{\text{pop}}}\} \tag{25}$$

where $\boldsymbol{B}$ is a 9×9 matrix and represents the prime electrical connection state of the PV arrays. n_{pop} is the number in the population.

In the process of PV array reconstruction, each PV array only exchanges its row with another array in the same column. Therefore, the optimization variables should meet the following constraints:

$$\begin{cases} x_{pq} \in \{1,2,\ldots,9\}, p = 1,2,\ldots,9; q = 1,2,\ldots,9 \\ \bigcup_{p=0}^{9} x_{pq} = \{1,2,\ldots,9\}, q = 1,2,\ldots,9 \end{cases} \tag{26}$$

where x_{pq} is the electrical connection state of PV arrays at the pth row and the qth column. To satisfy the constraints in (25), a MATLAB function 'randperm (n)' is introduced as:

$$\begin{cases} \boldsymbol{B}_q = \text{randperm}(9), q = 1,2,\ldots,9 \\ \boldsymbol{B} = \left[\boldsymbol{B}_1, \boldsymbol{B}_2, \ldots, \boldsymbol{B}_q, \ldots, \boldsymbol{B}_9\right] \end{cases} \tag{27}$$

where 'randperm (9)' means to randomly sort 9 data in a column, and $\boldsymbol{B}_q$ represents the qth column of the $\boldsymbol{B}$.

(B) Discretization for optimization process.

In order to adapt the optimization method to the reconfiguration of the PV array, the electrical connection status of each PV array is reallocated as:

$$s_{pq} = \mathrm{rank}(x_{pq}, \boldsymbol{x}_q) \tag{28}$$

where $\boldsymbol{x}_q = [X_1, X_2, \ldots, X_i, \ldots, X_9]$ denotes the solution vector of arrays at the qth column, and $\mathrm{rank}(x_{pq}, \boldsymbol{x}_q)$ denotes the order of x_{pq} among all solutions $\boldsymbol{x}_q$, and is set in ascending order.

4 Design of DLCI-I and DLCI-II based TCT PV array reconfiguration

The existence of PSC will cause a huge output power mismatch loss in PV power plants, resulting in greatly reduced output power. This will seriously affect the power generation and revenue of the entire PV enterprise. Therefore, there is an urgent need to find a method of reconstructing the PV system to reduce the impact of PSC [33]. This paper proposes a PV array reconfiguration (OAR) model based on electrical switches. This is used to reconfigure array positions to improve power generation output efficiency [34, 35]. The main steps are as follows: first, for the OAR model, the DLCI is used for discrete optimization to obtain the best electrical connection state. Then, the positions of the PV arrays are changed according to the electrical signals of the switch matrix to meet the required electrical connection state. The model proposed in this paper requires many electrical switches to meet the requirements of different states, and therefore, in order to reduce the switch cost and later maintenance cost, an electrical switch design is proposed as shown in Fig. 4. The end point of the electrical switch on the left can exchange the position of the rows in each column of the PV array. After reconfiguration, the connection between adjacent rows can be realized through the right bus.

Figure 5 shows the control structure diagram of the TCT PV array reconfiguration based on DLCI-I and DLCI-II. The reconfiguration of the position of PV arrays based on the optimal PV array reconfiguration model [23] is proposed in this work. First, the best electrical connection state can be obtained by discrete optimization based on the DLCI-I and DLCI-II OAR models. Then the physical positions of PV.

arrays are rearranged through electrical switches according to the obtained connection state to ensure that PV arrays can operate optimally in various PSCs [36, 37].

The purpose of reconfiguring PV arrays is to guarantee that the entire PV power plant can obtain the maximum output power in various PSCs. Therefore, its objective function can be modelled as:

$$f = \max P(C) = \max(n \times I_{\mathrm{D}}(C) \times V_{\mathrm{D}}(C)) \tag{29}$$

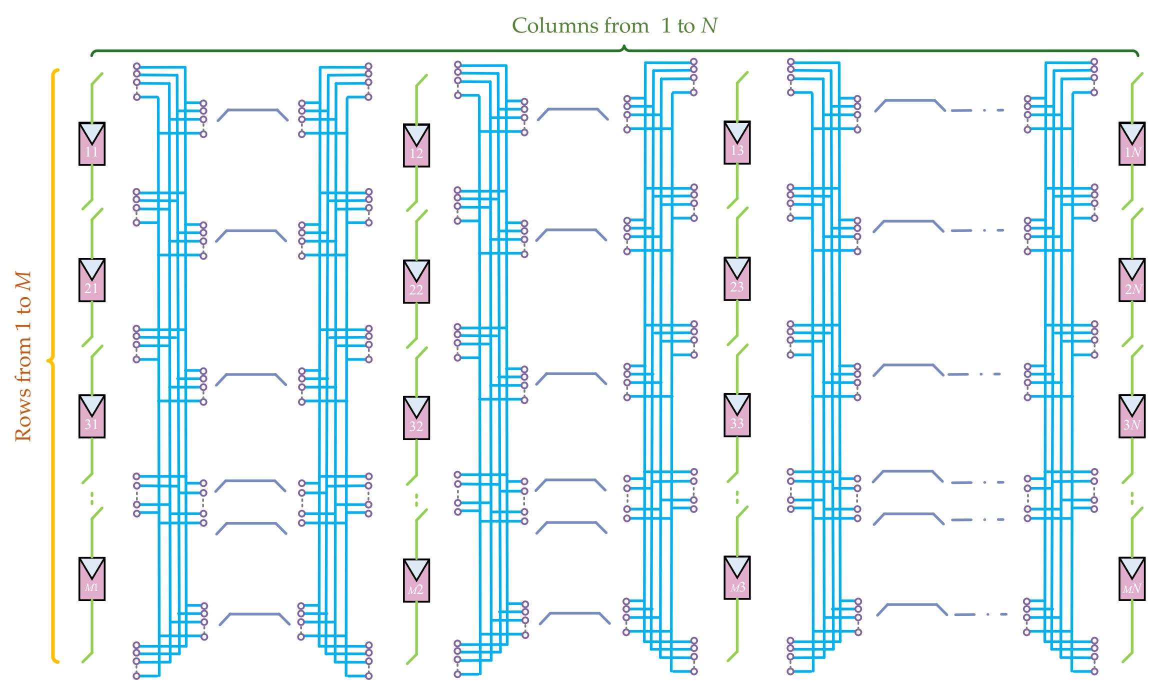

Fig. 4 Configuration of electrical switching arrangement

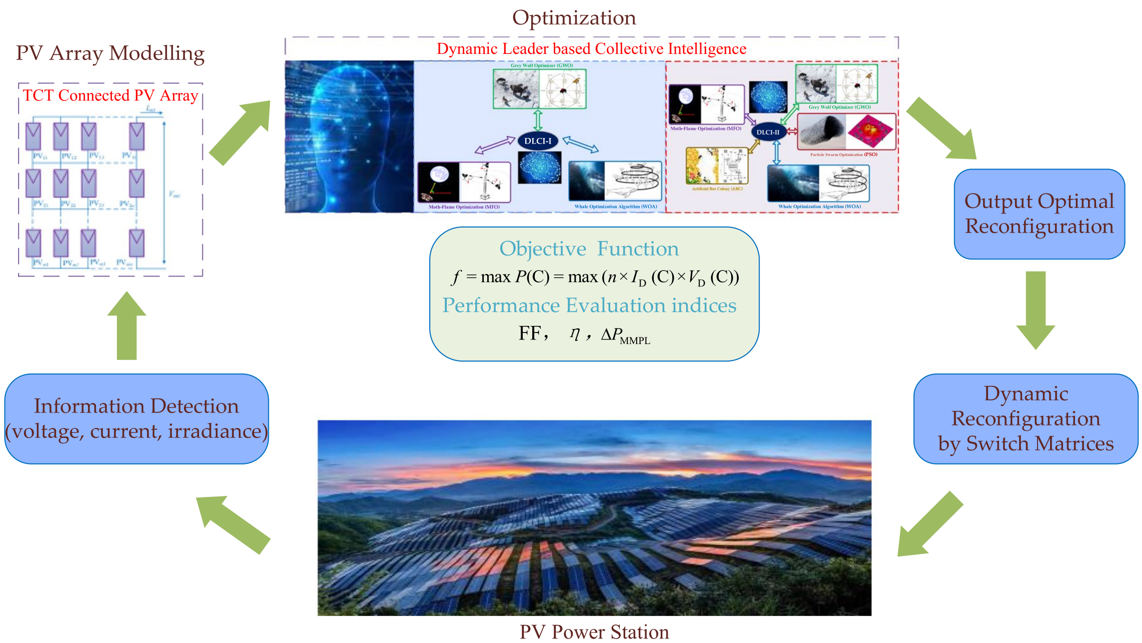

Fig. 5 The control structure diagram of DLCI-I and DLCI-II based TCT PV array reconfiguration

where $P(\mathrm{C})$ is the output power of the PV power plant at the C^{th} case of PSC, n is the number of subsystems of the PV power plant. Figure 6 represents the executive procedure of the process of PV reconstruction by the algorithm.

5 Case study

5.1 Operating conditions setting

Here 10 cases of PSCs are designed to verify the superior performance of PV array reconfiguration based on DLCI-I and DLCI-II algorithms. It is worth noting that the designed PSCs are simulations that comprehensively consider the occlusion effects caused by trees, buildings, bird droppings, rain, snow, and dust in practical engineering application. Each irradiation intensity is represented by a different color block, as shown in Fig. 7. The PV power plant simulated consists of 20 identical PV arrays. Each PV array is connected in a 9 × 9 TCT configuration. Table 1 gives the electrical characteristics of each PV module. To verify the effectiveness of DLCI-I and DLCI-II for PV array reconfiguration, their performance is compared with their respective sub-optimizers. Also, two algorithms (GA and BOA) are considered as competitive algorithms for comparison. Table 2 shows the parameters of all optimization algorithms. In addition, the maximum number of iterations $k_{\max}$ and population numbers n_{pop} of all algorithms are uniformly set to 200 and 50 to ensure fairness and reliability for performance comparison. Because DLCI-I and DLCI-II and their respective comparison algorithms are heuristic, their application in practical engineering will inevitably be affected by their own inherent defects (randomness), i.e., the results obtained with each optimization are not always the same. To avoid this shortcoming and obtain the global optimal solution, 30 runs of all algorithms are performed on MATLAB/Simulink 2021b. The applied solver is ode23 with a fixed-step size of 10^{-3} s. A fairer conclusion is given by comparing the maximum value and average value of power based on 30 runs.

Figure 8 presents the P–V and I–V curves of the 9×9 PV arrays in 10 cases of PSCs. It can be seen that the P–V curve of the PV array in the 10th case of PSC has the largest number of peaks. There is no doubt that the PV array is prone to power oscillation in the 10th case of PSC, resulting in large power mismatch loss. Therefore, the next simulation study will focus on this PSC to verify the PV array reconfiguration performance of DLCI-I and DLCI-II for the 10th case of PSC.

5.2 Result analysis of DLCI-I for PV array reconfiguration

Table 3 presents the optimization results obtained by DLCI-I, its sub-optimizer algorithm, and competitive algorithms applied for PV array reconfiguration in 10 cases of PSCs to extract maximum output power. $P_{\max}$ and P_{mean} represent the maximum and mean values of output power obtained by the optimization algorithm in 30 independent runs. It can be seen from Table 3 that the PV array reconstruction based on DLCI-I obtains the optimal $P_{\max}$ and P_{mean} (in bold). To further evaluate the optimization performance of DLCI-I, three evaluation

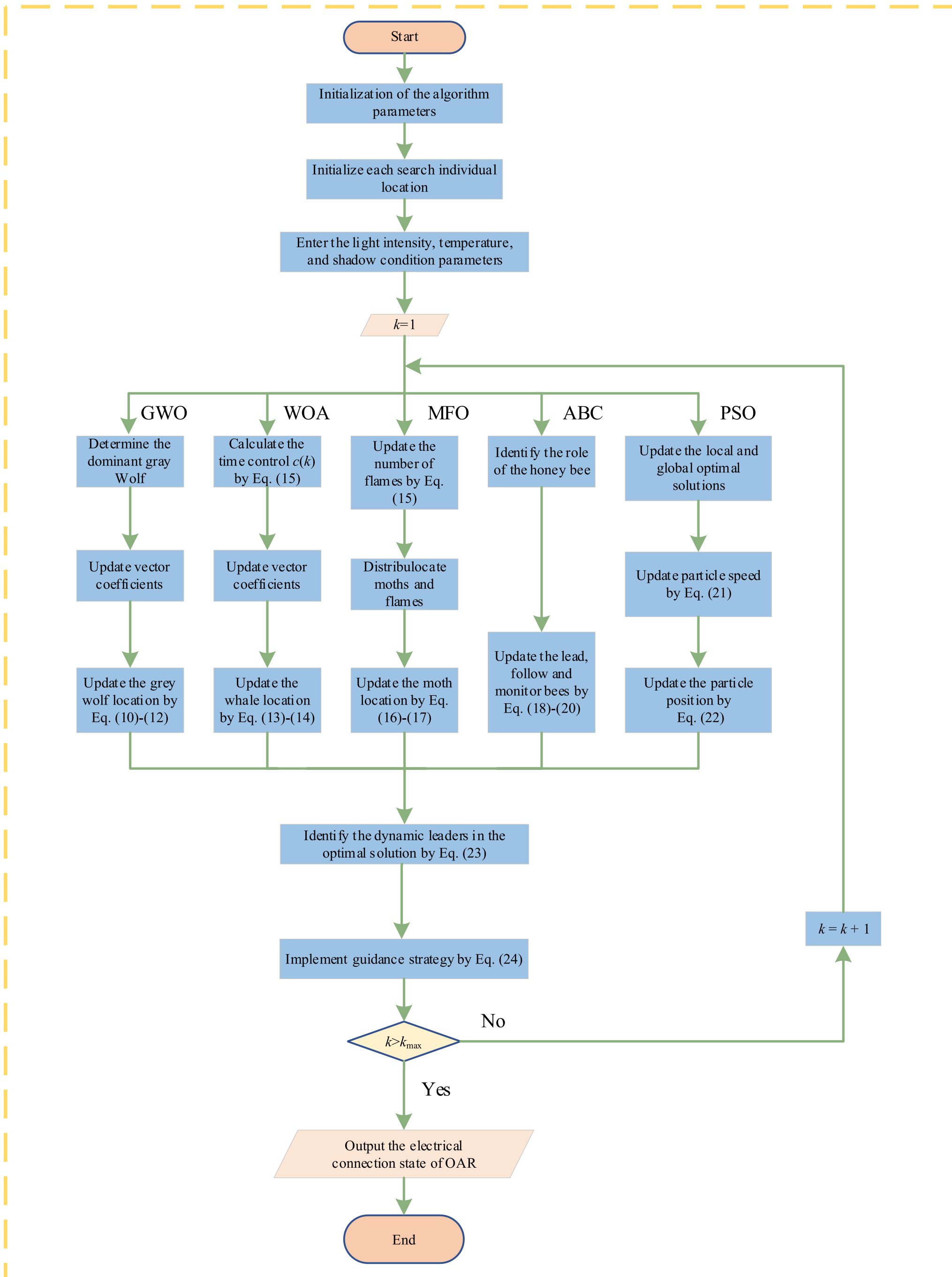

Fig. 6 Overall execution procedure of DLCI for PV array reconfiguration

indicators are introduced, namely, FF, ΔP_{MMPL} and η. The calculation of the three indicators depends on the total P_{mean} of 10 cases of PSCs. It can be clearly seen that the FF and η obtained by DLCI-I are the largest and ΔP_{MMPL} is the smallest compared to its sub-optimizer algorithm. The FF obtained by DLCI-I are 2.42%, 0.29%, 0.24%, 7.43%, 8.00% higher than those from GWO, WOA, MFO, GA, and BOA, respectively. For ΔP_{MMPL}, it is 5.13%, 1.21%, 1.01%, 0.24% and 1.18% lower than those from GWO, WOA, MFO, GA, and BOA, respectively.

Figure 9 gives the optimal reconfiguration solution for 9×9 PV arrays based on DLCI-I. It can be seen that the concentrated shading of all PV arrays presented in Fig. 9 is redistributed to different rows. Figure 10

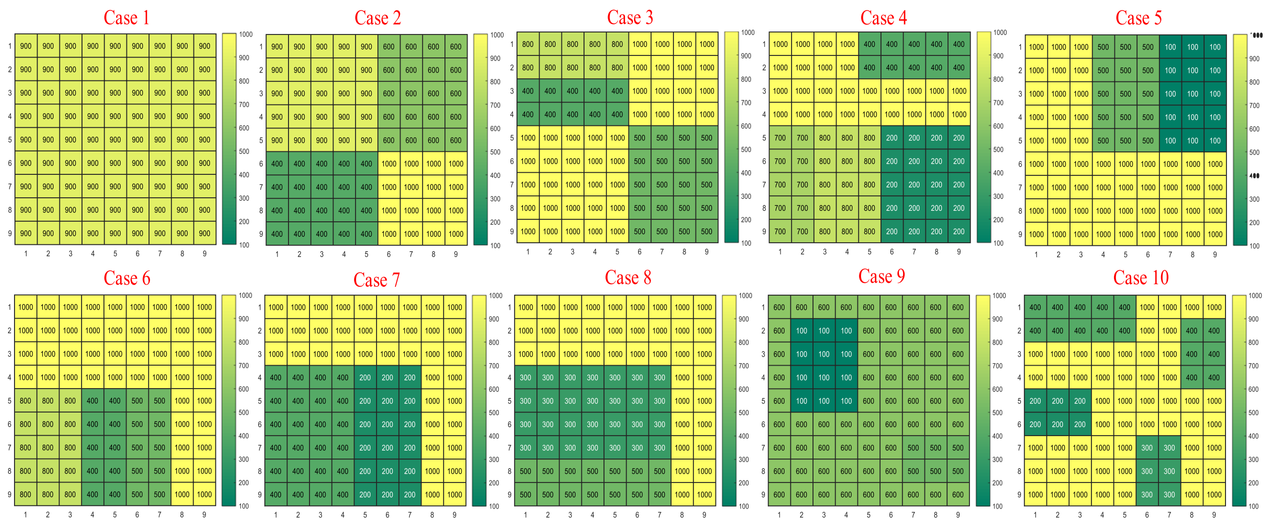

Fig. 7 The irradiation distribution of the 9 × 9 PV arrays in 10 cases of PSCs

Table 1 Electrical characteristics of each PV module

Parameter	Value
Number of cells	60
Open circuit voltage	36.24 V
Current of maximum power point	7.44 A
Short-circuit current	8.04 A
Maximum output power	224.98 W
Voltage of maximum power point	30.24 V

Table 2 Parameters of all optimization algorithms

Sub-optimizer	Parameters	Value
GWO [25]	Linearly decreased coefficient a	$2-1*(2/k_{max})$
	Coefficient vector A	$2*a*rand(0,1)-a$
	Coefficient vector C	$2*rand(0,1)$
WOA [26]	Log-helix shape constant b	1
	Coefficient vector A	$2*a*rand(0,1)-a$
	Coefficient vector C	$2*rand(0,1)$
MFO [27]	Log-helix shape constant b	1
ABC [28]	Maximum number of honey source for single preservation n	1
	Honey source search range expansion coefficient a	1
PSO [19]	Cognitive constant c_1	0.5
	Social constant c_2	0.7
	Inertia weight ∞	$0.96-k/k_{max}$
GA [18]	Probability of crossover P_c	0.8
	Probability of mutation P_m	0.05
BOA [20]	Probability switch p	0.6
	Initial sensory modality c_0	0.01
	Initial power exponent α_0	0.1

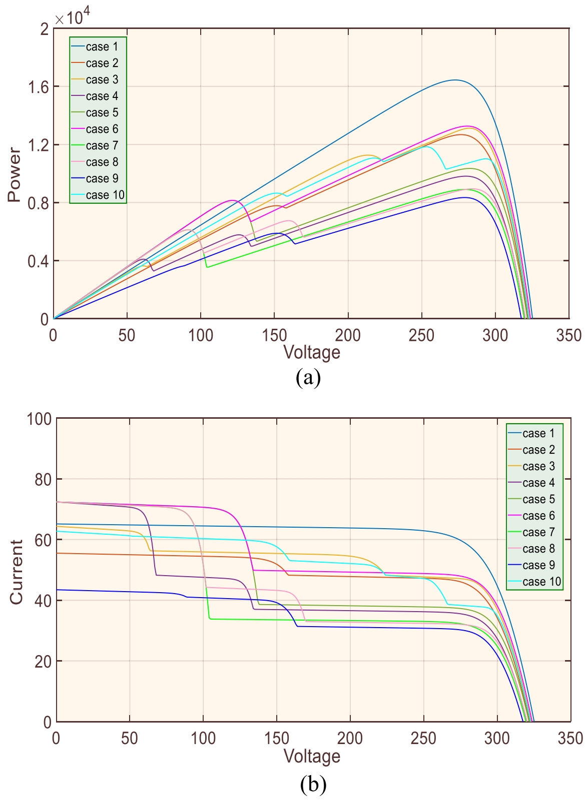

Fig. 8 Output results of the 9×9 PV arrays in 10 cases of PSCs. **a** *P–V* curves, and **b** *I–V* curves

presents the *P–V* and *I–V* curves of the 9×9 PV arrays reconfigured by DLCI-I in the 10th case of PSC. Compared with without optimization, the output power of the PV arrays obtained based on DLCI-I is improved by 16.86%. Furthermore, the number of power peaks in the *P–V* curve of the PV arrays obtained by DLCI-I is significantly reduced.

5.3 Analysis of DLCI-II for PV array reconfiguration

Table 4 provides the optimization results acquired by DLCI-II, its 5 sub-optimizer algorithms, and competitive algorithms for PV array reconfiguration in 10 cases of PSCs in 30 runs. One can see clearly from Table 4 that DLCI-II still has the optimal P_{max} and P_{mean} compared to other contrasting algorithms. Also, the FF and η acquired by DLCI-II are also the largest, while ΔP_{MMPL} generated by DLCI-II is the smallest.Particularly, the FF obtained by DLCI-II is 2.72%, 0.84%, 0.74%, 0.43%, 1.54%, 7.59% and 8.16% higher than those of GWO, WOA, MFO, ABC, PSO, GA, and BOA, respectively, while ΔP_{MMPL} is 94.2%, 98.12%, 98.32%, 99.00%, 96.61%, 99.07% and 98.15% of those from GWO, WOA, MFO, ABC, PSO, GA, and BOA, respectively.

The optimal reconfiguration solution of the 9×9 PV arrays reconfigured gained by DLCI-II is provided in Fig. 11. It can be clearly seen that the concentrated shading of all PV arrays shown in Fig. 11 is redistributed to different rows. This dramatically increases the output power of the PV plant. Figure 12 shows that in the 10th case of PSC, the maximum output power of PV arrays acquired by DLCI-II is 17.52% higher than that without optimization. Also, it can be clearly seen that the *P–V* curve produced by DLCI-II applied to the PV array reconfiguration has only a single power peak.

5.4 Result statistics

The mismatch power loss (ΔP_{MMPL} is an extremely important indicator to measure the optimization performance of the proposed algorithm applied to PV array reconfiguration. Figure 13 presents the total ΔP_{MMPL} obtained by DLCI-I, DLCI-II and their sub-optimizer algorithms for OAR in 10 cases of PSCs in 30 independent runs. It can be clearly seen that the total ΔP_{MMPL} acquired by DLCI-I and DLCI-II are significantly smaller than those from the single meta-heuristic algorithm. In addition, it can be found that the increase of the number of sub-optimizers has a certain effect on the improvement of DLCI optimization performance, but the effect is not significant. The total ΔP_{MMPL} acquired by DLCI-II is only 0.67% lower than that of DLCI-I.

6 Hardware-in-the-loop test

To further test the real-time output characteristics of the PV array at different irradiances and temperature, hardware-in-the-loop experiments are carried out based on the RTLAB platform. At a standard temperature of 25 ℃, the output characteristics of the PV array on the MATLAB and RTLAB platforms at different irradiances are shown in Fig. 14.The simulation experiments based on the MATLAB platform are conducted on Intel (R) Core (TM) i10-8401 CPU@4.20 GHz and 16 GB RAM. The solver of the MATLAB platform is selected as ode23 with a 10^{-3} s fixed-step size. From the output characteristic curves of the PV arrays on the two platforms in Figs. 15 and 16, it is clear that the experimental results based on the RTLAB platform are very similar to those based on the MATLAB platform, and thus subsequent cases can be conducted based on the MATLAB platform.

7 Discussion

It is worth noting that different meta-heuristic algorithms might be suitable for different optimization tasks because of their inherent property of high randomness. Hence this work tested 10 meta-heuristic algorithms, include GA, GWO, WOA, MFO, ABC, PSO, BOA, jellyfish

Table 3 Optimization results of OAR in 10 cases of PSCs in 30 runs of six algorithms

Case	GWO		WOA		MFO	
	P_{max} (kW)	P_{mean} (kW)	P_{max} (kW)	P_{mean} (kW)	P_{max} (kW)	P_{mean} (kW)
1	492.043	492.043	492.043	492.043	492.043	492.043
2	382.700	372.778	382.700	378.853	382.700	382.093
3	406.999	400.114	413.074	409.428	413.074	412.871
4	340.178	330.944	346.253	341.595	346.253	340.016
5	376.626	375.829	382.700	378.313	376.626	376.626
6	437.372	428.867	443.446	438.181	443.446	437.169
7	340.178	325.707	340.178	336.533	340.178	334.913
8	346.253	338.220	358.402	346.860	346.252	346.252
9	267.283	264.853	267.283	267.283	267.283	267.283
10	394.850	386.682	400.924	396.402	400.924	399.641
FF (Total)	52.48%		53.46%		53.51%	
ΔP_{MMPL} (Total) (kW)	1750.97		1681.52		1678.10	
η	67.97%		69.24%		69.30%	

Case	GA		BOA		DLCI-I	
	P_{max} (kW)	P_{mean} (kW)	P_{max} (kW)	P_{mean} (kW)	P_{max} (kW)	P_{mean} (kW)
1	492.043	492.043	492.043	492.043	492.043	492.043
2	382.701	381.391	388.775	387.965	388.775	382.498
3	419.148	414.734	413.074	412.264	419.148	413.276
4	352.327	352.327	346.253	343.013	346.253	342.000
5	400.924	386.089	382.701	382.309	400.924	379.163
6	449.521	442.029	443.447	443.244	443.446	439.396
7	340.178	340.178	340.178	338.963	340.178	338.963
8	358.402	355.567	358.402	354.757	358.402	350.100
9	267.283	267.283	267.283	267.283	267.283	267.283
10	405.379	400.708	396.875	369.689	400.924	400.789
FF (Total)	46.32%		45.75%		53.75%	
ΔP_{MMPL} (Total) (kW)	1665.12		1680.94		1661.09	
η	61.09%		60.35%		69.62%	

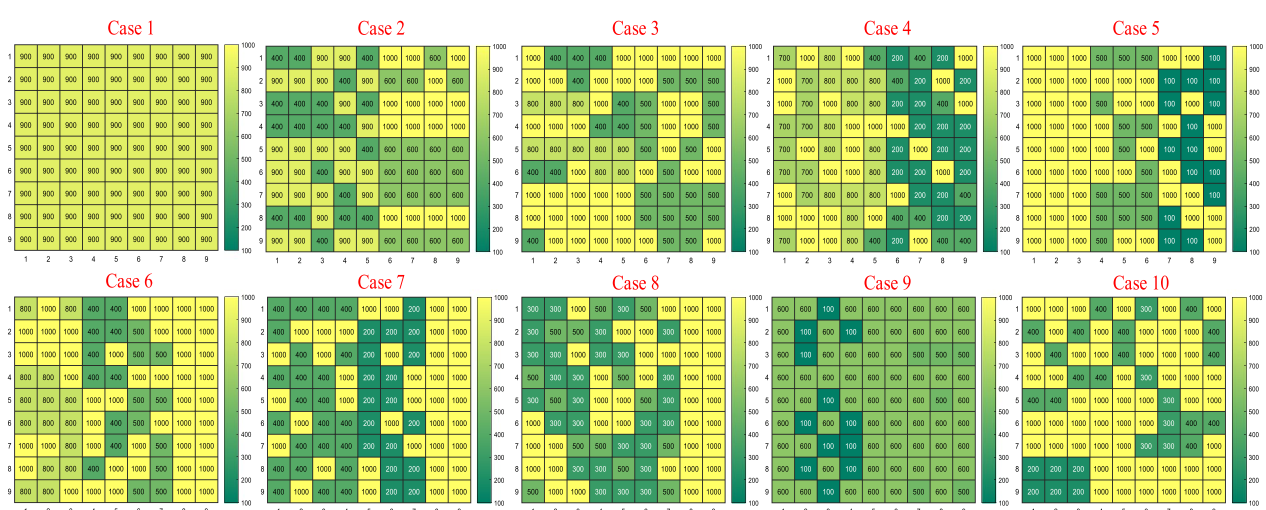

Fig. 9 The optimal solution of the 9×9 PV arrays reconfigured by DLCI-I with 10 cases of PSCs

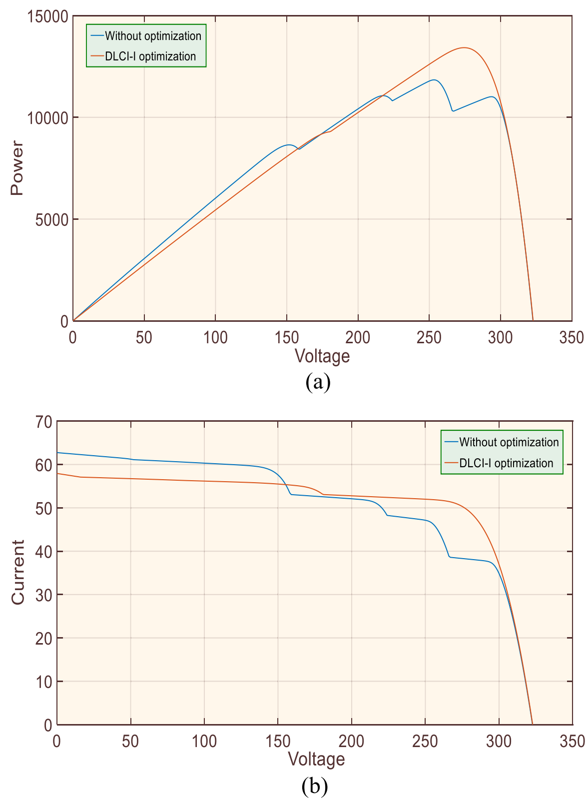

Fig. 10 Comparison result of PV arrays acquired without optimization and DLCI-I in the 10th case of PSC. **a** *P–V* curves, and **b** *I–V* curves

search algorithm (JSA) [38], ant colony algorithm (ACO) [39], and simulated annealing (SA) [40], as possible candidates to synthesize DLCI. After trial-and-error, the best five algorithms are chosen, i.e., GWO, WOA, MFO, ABC, and PSO. The novelty of this work can be summarized as follows:

- Various meta-heuristic algorithms have been employed as sub-optimizers to dynamically seek the global optimum of PV system reconfiguration. This shows that DLCI significantly outperforms the individual sub-optimizers while the increase of number of sub-optimizers has a relatively small impact on overall DLCI optimization performance.
- Generally speaking, PV system reconstruction is a discrete optimization associated with a limited number of solutions. These can be efficiently resolved by conventional meta-heuristic algorithms. Meta-heuristic algorithms usually own high randomness in solving a given problem, e.g., some algorithms perform well for some problems but not for others, and they also vary as to their improvement/modification. Hence, the improvement of meta-heuristic algorithms cannot guarantee an improvement of optimization performance or may even degrade it.
- PV reconfiguration requires real-time data collection and online reconfiguration. These require an efficient computation speed. In this work, 10 different algorithms have been tested and the best have been chosen to incorporate DLCI. Such a framework already increases the overall algorithm structure complexity and possible further improvement of them may noticeably increase the overall computation burden.
- Finally, a hardware-in-the-loop experiment has been carried out to validate the hardware implementation feasibility of the proposed DLCI.

8 Conclusions

This paper proposes a novel PV array reconfiguration method by means of a dynamic leader-based collective intelligence for maximum power extraction of PV systems in various PSCs, and the main innovations and value are:

(1) First, a series of discrete operation improvements are made to the DLCI, so that DLCI with continuous optimization performance has stronger universality. This can be used to solve not only continuous optimization problems but also any discrete optimization problems.
(2) The idea of the DLCI is innovatively used to solve the problem of PV array reconfiguration in various PSCs, and two structures of DLCI (DLCI-I and DLCI-II) are designed to verify the influence of the number of sub-optimizers on its optimization performance. The results show that the increase of the number of sub-optimizers has a certain but limited effect on the improvement of optimization performance.
(3) Taking into account the effects of shadows from clouds, trees, buildings and dust accumulation, bird droppings, snow, etc., 10 cases of discrete PSCs are designed. The study shows that the DLCI with multiple sub-optimizer search mechanisms can achieve a deeper local search and a wider global search with minimal ΔP_{MMPL}.

However, the reconstruction method proposed in this paper still has some limitations:

(1) Strong randomness is a common problem of heuristic algorithms. For PV power stations of different sizes, it is necessary to set the number of populations and iterations of the sub-optimizers to weigh

Table 4 Optimization results of OAR in 10 cases of PSCs in 30 runs of eight algorithms

Case	GWO		WOA		MFO		ABC	
	P_{max} (kW)	P_{mean} (kW)	P_{max} (kW)	P_{mean} (kW)	P_{max} (kW)	P_{mean} (kW)	P_{max} (MW)	P_{mean} (MW)
1	492.043	492.043	492.043	492.043	492.043	492.043	492.043	492.043
2	382.700	372.778	382.700	378.853	382.700	382.093	382.700	381.485
3	406.999	400.114	413.074	409.428	413.074	412.871	413.074	411.048
4	340.178	330.944	346.253	341.595	346.253	340.016	346.253	343.215
5	376.626	375.829	382.700	378.313	376.626	376.626	382.700	379.352
6	437.372	428.867	443.446	438.181	443.446	437.169	443.446	439.599
7	340.178	325.707	340.178	336.533	340.178	334.913	340.178	340.178
8	346.253	338.220	358.402	346.860	346.252	346.252	358.402	347.467
9	267.283	264.853	267.283	267.283	267.283	267.283	267.283	267.283
10	394.850	386.682	400.924	396.402	400.924	399.641	400.924	398.899
FF (Total)	52.48%		53.46%		53.51%		53.68%	
ΔP_{MMPL} (Total) (kW)	1750.97		1681.52		1678.10		1666.45	
η	67.97%		69.24%		69.30%		69.52%	

Case	PSO		GA		BOA		DLCI-II	
	P_{max} (MW)	P_{mean} (MW)	P_{max} (kW)	P_{mean} (kW)	P_{max} (kW)	P_{mean} (kW)	P_{max} (MW)	P_{mean} (MW)
1	492.043	492.043	492.043	492.043	492.043	492.043	492.043	492.043
2	388.775	374.438	382.701	381.391	388.775	387.965	388.775	383.712
3	413.074	405.662	419.148	414.734	413.074	412.264	419.148	414.490
4	346.253	337.167	352.327	352.327	346.253	343.013	352.327	344.632
5	382.7	375.842	400.924	386.089	382.701	382.309	400.924	381.634
6	443.446	436.359	449.521	442.029	443.447	443.244	449.521	439.801
7	340.178	330.863	340.178	340.178	340.178	338.963	340.178	340.178
8	346.253	344.241	358.402	355.567	358.402	354.757	358.402	352.357
9	267.283	266.675	267.283	267.283	267.283	267.283	267.283	267.283
10	400.924	395.862	405.379	400.708	396.875	369.689	402.544	400.951
FF (Total)	53.09%		46.32%		45.75%		53.91%	
ΔP_{MMPL} (Total) (kW)	1707.86		1665.12		1680.94		1649.93	
η	68.76%		61.09%		60.35%		69.82%	

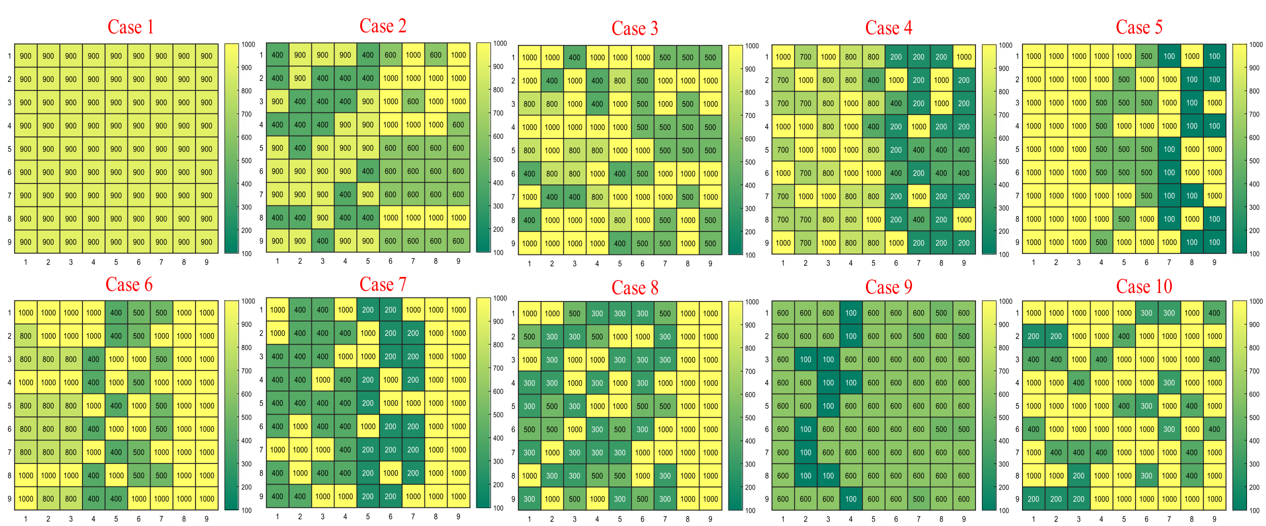

Fig. 11 The optimal solution of the 9×9 PV arrays reconfigured by DLCI-II with 10 cases of PSCs

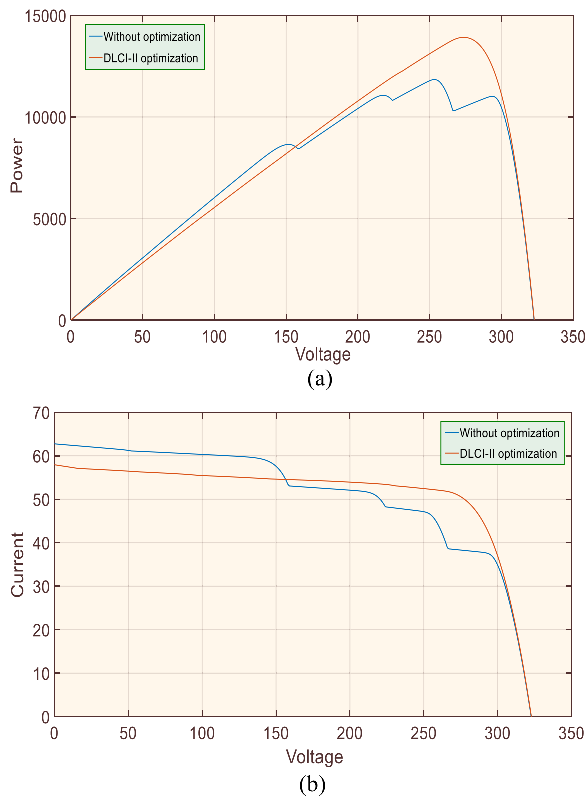

Fig. 12 Comparison result of PV arrays acquired by without optimization and DLCI-II in the 10th case of PSC. **a** *P–V* curves, and **b** *I–V* curves

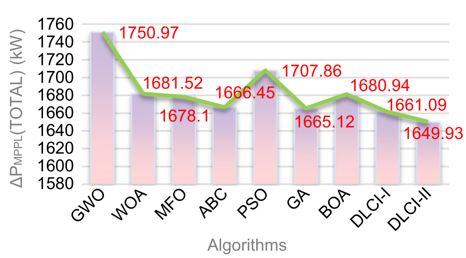

Fig. 13 Total mismatched power loss (ΔP_{MMPL}) of OAR acquired by six algorithms in 10 cases of PSCs in 30 runs

the quality of the algorithm. The DLCI has complex parameter adjustment that needs to be improved.

(2) The reconstruction technology of a PV array is mainly designed for a change of environment. In the reconstruction scheme proposed in this paper, the influence of the shelter on the PV system is mainly considered.

Future research will focus on the following aspects:

(1) Hardware experiments of AOA-based MPPT for centralized TEG systems under DTG to further verify the practical feasibility of the technique.

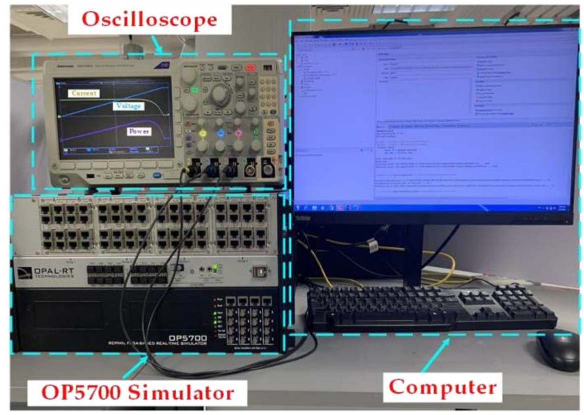

Fig. 14 Physical picture of hardware-in-the-loop test

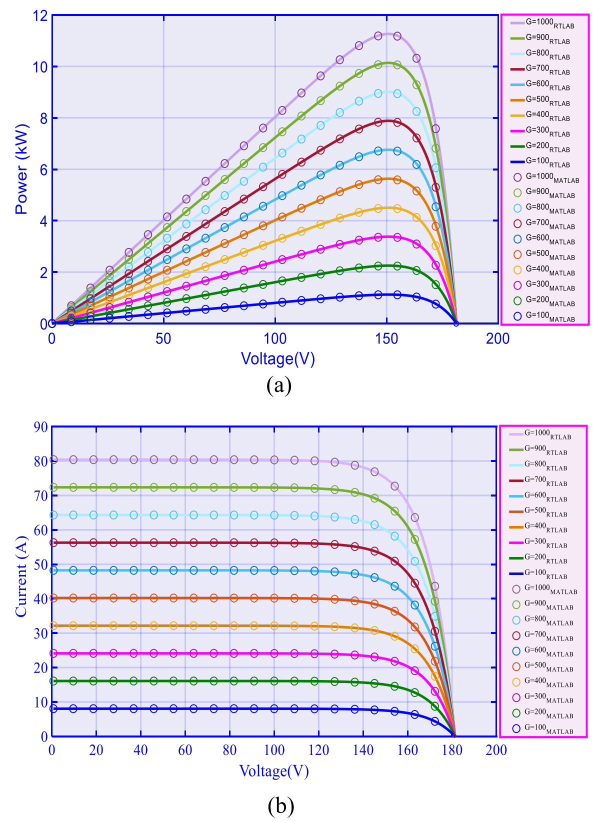

Fig. 15 Output characteristics of each photovoltaic array at 25 ℃. **a** *I–V* curves and **b** *P–V* curves

(2) AOA applied to other energy conversion optimization problems, such as PV system MPPT in a PSC.

(3) In the follow-up work, the reconstruction effect in different conditions needs to be further considered.

(4) PV reconstruction technology is an important part of renewable energy power generation technology, which has certain guidance and reference value for

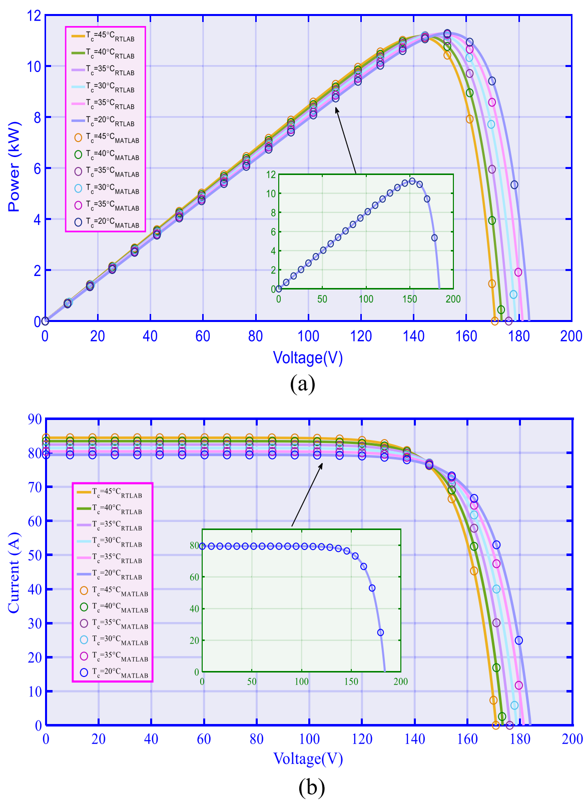

Fig. 16 Output characteristic of each PV array acquired at various temperatures. **a** *I*–*V* curves and **b** *P*–*V* curves

the reconstruction of other power generation technologies. Therefore, the reconstruction technology of thermoelectric power generation will be examined in subsequent work.

List of symbols

Variables

V_{ap}	Maximum voltage at the *p*th row
I_{pq}	Output current of PV arrays
V_D	Output voltage of PV array system
I_D	Sum of current across each column of PV array
$\vec{X}_{\alpha}$	Position vectors of α wolf
$\vec{X}_{\beta}$	Position vectors of β wolf
$\vec{X}_{\delta}$	Position vectors of δ wolf
N_f	The number of flames
$\vec{F}_j$	Position vector the flame
p_i	Probability of the *i*th bee being selected
$\vec{V}_i$	Velocity vector of the *i*th particle
$\vec{P}_i$	Best position of the particle
$\vec{G}$	The global best position
L	Dynamic leader
f_o^{best}	The fitness function of the *o*th sub-optimizer
$\vec{X}_o^{worst}$	The poor solution obtained by the *o*th suboptimizer
$\vec{X}_L^{best}$	The optimal solution obtained by the dynamic leader
x_{pq}	The electrical connection state
s_{pq}	The sequence of solutions
x_q	The solution vector of arrays

Abbreviations

ABC	Artificial bees colony
DLCI	Dynamic leader-based collective intelligence
GMPP	Global maximum power point
GWO	Grey wolf optimizer
MPPT	Maximum power point tracking
MFO	Moth-flame optimization
OAR	Photovoltaic array reconfiguration
PV	Photovoltaic
PSC	Partial shading condition
PSO	Particle swarm optimization
TCT	Total-cross-tied
WOA	Whale optimization algorithm

DLCI parameters

k_{max}	Maximum iteration number
n	Number of sub-optimizers
n_{pop}	Population size

Performance evaluation

FF	Fill factor
ΔP_{MMPL}	Mismatched power loss
η	Efficiency

Acknowledgements
This work was supported by National Natural Science Foundation of China (62263014, 62263014) and Yunnan Provincial Basic Research Project (202201AT070857).

Author contributions
First, a series of discrete operation improvements are made to the DLCI, so that DLCI with continuous optimization performance has stronger universality, which can not only be used to solve continuous optimization problems, but also can be used to solve any discrete optimization problem; The idea of DLCI is innovatively used to solve the problem of PV array reconfiguration under various PSCs, and two structures of DLCI (DLCI-I and DLCI-II) are designed to verify the influence of the number of sub-optimizers on its optimization performance. The research results show that the increase of the number of sub-optimizers has a certain effect on the improvement of optimization performance, but the effect is not very significant; Taking into account the effects of shadows from clouds, trees, buildings and dust accumulation, bird droppings, snow, etc. 10 cases of discrete PSCs are designed. The study shows that DLCI with multiple sub-optimizer search mechanisms can achieve a deeper local search and a wider global search with minimal ΔP_{MMPL}.

Funding
National Natural Science Foundation of China (61963020,62263014); Yunnan Provincial Basic Research Project (202201AT070857).

Availability of data and materials
The datasets used or analyzed during the current study are available from the corresponding author on reasonable request.

Declarations

Competing interests
The authors declare that they have no known competing financial interests or personal relationships that could have appeared to influence the work reported in this paper.

Received: 23 December 2022 Accepted: 9 August 2023
Published online: 30 August 2023

References

1. Yang, B., Li, Y., Li, J., Shu, H., Zhao, X., Ren, Y., & Li, Q. (2022). Comprehensive summary of solid oxide fuel cell control: A state-of-the-art review. *Protection and Control of Modern Power Systems, 7*(36), 1–31.
2. Yang, B., Liu, B. Q., & Zhou, H. Y. (2022). A critical survey of technologies of large offshore wind farm integration: Summarization, advances, and perspectives. *Protection and Control of Modern Power Systems, 7*(17), 1–32.
3. Pillai, D. S., Ram, J. P., Nihanth, M. S. S., et al. (2018). A simple, sensorless and fixed reconfiguration scheme for maximum power enhancement in PV systems. *Energy Conversion and Management, 172*, 402–417.
4. Yang, B., Wang, J. B., Zhang, X. S., et al. (2020). Comprehensive overview of meta-heuristic algorithm applications on PV cell parameter identification. *Energy Conversion and Management, 208*, 112595.
5. Chen, Y. J., Yang, B., Guo, Z. X., et al. (2022). Dynamic reconfiguration for TEG systems under heterogeneous temperature distribution via adaptive coordinated seeker, Protection and Control of. *Modern Power Systems, 3*, 567–585.
6. Kumar, D. S., Savier, J. S., & Biju, S. S. (2020). Micro-synchrophasor based special protection scheme for distribution system automation in a smart city. *Protection and Control of Modern Power Systems, 5*(1), 97–110.
7. Erdiwansyah, E., Mahidin, M., Husin, H., & Zaki, M. (2021). A critical review of the integration of renewable energy sources with various technologies. *Protection and Control of Modern Power Systems, 6*(1), 37–54.
8. Desai, A. A., & Mikkili, S. (2020). Novel hybrid PV array configurations for extracting maximum power by reducing number of peaks and mitigating mismatching power loss under partial shading conditions. In *IECON 2020 The 46th annual conference of the IEEE industrial electronics society*, Singapore (pp. 1872–1877).
9. Shang, L. Q., Guo, H. C., & Zhu, W. W. (2020). An improved MPPT control strategy based on incremental conductance algorithm. *Protection and Control of Modern Power Systems, 5*(2), 176–184.
10. Sreekantha, S. R., & Chandrasekhar, Y. (2020). Odd-even-prime pattern for PV array to increase power output under partial shading conditions. *Energy, 213*, 118780.
11. Fathy, A., Rezk, H., & Yousri, D. (2020). A robust global MPPT to mitigate partial shading of triple-junction solar cell-based system using manta ray foraging optimization algorithm. *Solar Energy, 207*, 305–316.
12. Yang, B., Shao, R. N., Zhang, M. T., et al. (2021). Socio-inspired democratic political algorithm for optimal PV array reconfiguration to mitigate partial shading. *Sustainable Energy Technologies and Assessments, 48*, 101627.
13. Yang, B., Zhu, T. J., Wang, J. B., et al. (2020). Comprehensive overview of maximum power point tracking algorithms of PV systems under partial shading condition. *Journal of Cleaner Production, 268*, 121983.
14. Ajmal, A. M., Babu, T. S., Ramachandaramurthy, V. K., et al. (2020). Static and dynamic reconfiguration approaches for mitigation of partial shading influence in PV arrays. *Sustainable Energy Technologies and Assessments, 40*, 100738.
15. Woyte, A., Nijs, J., & Belmans, R. (2003). Partial shadowing of photovoltaic arrays with different system configurations. *Literature review and field test results, Solar Energy, 74*(3), 217–233.
16. Rao, P. S., Ilango, G. S., & Nagamani, C. (2014). Maximum power from PV arrays using a fixed configuration under different shading conditions. *IEEE Journal of Photovoltaics, 4*(2), 679–686.
17. Dhanalakshmi, B., & Rajasekar, N. (2018). A novel competence square based PV array reconfiguration technique for solar PV maximum power extraction. *Energy Conversion and Management, 174*, 897–912.
18. Yang, B., Ye, H. Y., Wang, J. B., et al. (2021). PV arrays reconfiguration for partial shading mitigation: Recent advances, challenges and perspectives. *Energy Conversion and Management, 247*, 114738.
19. Rajan, N. A., Shrikant, K. D., Dhanalakshmi, B., et al. (2017). Solar PV array reconfiguration using the concept of standard deviation and genetic algorithm. *Energy Procedia, 117*, 1062–1069.
20. Chen, P. Y., Chao, K. H., & Liao, B. J. (2018). Joint operation between a PSO-based global MPP tracker and a PV module array configuration strategy under shaded or malfunctioning conditions. *Energies, 11*(8), 1–16.
21. Ramaprabha, R., & Mathur, B. L. (2012). A comprehensive review and analysis of solar PV array configurations under partial shaded conditions. *International Journal of Photoenergy, 2012*, 1–16.
22. Fathy, A. (2020). Butterfly optimization algorithm based methodology for enhancing the shaded PV array extracted power via reconfiguration process. *Energy Conversion and Management, 220*, 113115.
23. Ishaque, K., Salam, Z., Taheri, H., & Shamsudin, A. (2011). A critical evaluation of EA computational methods for photovoltaic cell parameter extraction based on two diode model. *Solar Energy, 85*(9), 1768–1779.
24. Yang, B., Yu, T., Zhang, X. S., et al. (2019). Dynamic leader based collective intelligence for maximum power point tracking of PV systems affected by partial shading condition. *Energy Conversion and Management, 179*, 286–303.
25. Zhang, X. S., Li, C. Z., Li, Z. L., et al. (2021). Optimal mileage-based PV array reconfiguration using swarm reinforcement learning. *Energy Conversion and Management, 232*, 113892.
26. Shubhankar, N. D., Sumedh, B. D., Jishnu, S. M., et al. (2015). Solar PV array reconfiguration under partial shading conditions for maximum power extraction using genetic algorithm. *Renewable and Sustainable Energy Reviews, 43*, 102–110.
27. Mirjalili, S., Mirjalili, S. M., & Lewis, A. (2014). Grey wolf optimizer. *Advances in Engineering Software, 69*, 46–61.
28. Mirjalili, S., & Lewis, A. (2016). The whale optimization algorithm. *Advances in Engineering Software, 95*, 51–67.
29. Mirjalili, S. (2015). Moth-flame optimization algorithm: A novel nature-inspired heuristic paradigm. *Knowledge-Based Systems, 89*, 228–249.
30. Xiang, W. L., Li, Y. Z., Meng, X. L., et al. (2017). A grey artificial bee colony algorithm. *Applied Soft Computing, 60*, 1–17.
31. Yousri, D., Babu, T. S., Beshr, E., et al. (2020). A robust Strategy based on marine predators algorithm for large scale photovoltaic array reconfiguration to mitigate the partial shading effect on the performance of PV system. *IEEE Access, 8*, 112407–112426.
32. Xi, L., Wu, J., Xu, Y., et al. (2019). Automatic generation control based on multiple neural networks with actor-critic strategy. *IEEE Transactions on Neural Networks and Learning Systems, 32*, 2483–2493.
33. Li, R., Wong, P., Wang, K., et al. (2019). Power quality enhancement and engineering application with high permeability distributed photovoltaic access to low-voltage distribution networks in Australia. *Protection and Control of Modern Power Systems, 5*, 183–189.
34. Bi, Z., Ma, J., Wang, K., et al. (2022). Identification of partial shading conditions for photovoltaic strings. *IEEE Access, 8*, 75491–75502.
35. Krishnan, G. S., Kinattingal, S., Simon, S. P., et al. (2020). MPPT in PV systems using ant colony optimisation with dwindling population. *IET Renewable Power Generation, 14*, 1105–1112.
36. Varma, G. K., Barry, V. R., Jain, R. K., et al. (2021). An MMTES algorithm for dynamic photovoltaic array reconfiguration to enhance power output under partial shading conditions. *IET Renewable Power Generation, 15*, 809–820.
37. Pillai, D. S., Ram, J. P., Nihanth, M. S. S., et al. (2018). A simple sensorless and fixed reconfiguration scheme for maximum power enhancement in PV systems. *Energy Conversion and Management, 172*, 402–417.
38. Yang, B., Zhang, M. T., Guo, Z. X., et al. (2023). Adaptive evolutionary jellyfish search algorithm based optimal photovoltaic array reconfiguration under partial shading condition for maximum power extraction. *Expert Systems with Applications, 215*, 119325.
39. Cao, R., Ding, Y., Fang, X., Liang, S., Qi, F., Yang, Q., & Yan, W. (2020). PV array reconfiguration under partial shading conditions based on ant colony optimization. In *2020 Chinese control and decision conference (CCDC)*, Hefei, China (pp. 703–708).
40. Krishna, G. S., & Moger, T. (2021). Enhanced power generation for total-cross-tied PV array using simulated annealing under partial shading conditions. *IET Renewable Power Generation, 14*(17), 3457–3468.